

Stokes Polarimetry Imaging of Rat-Tail Tissue in a Turbid Medium Using Incident Circularly Polarized Light

Paul J. Wu PhD and Joseph T. Walsh, Jr. PhD*

Biomedical Engineering Department, Northwestern University, Evanston, Illinois 60208

Background and Objectives: We describe a Stokes polarimetry imaging technique that quantifies the polarization properties of remitted light backscattered from a sample.

Study Design/Materials and Methods: Right- and left-circularly polarized near-infrared light was used to illuminate rat-tail tissue embedded in turbid gelatin.

Results: The degree of linear polarization (DoLP) and degree of circular polarization (DoCP) image-maps indicate that increasing the depth of the rat tail within the turbid medium and varying the rat-tail geometry and orientation relative to the light source affected the contrast between structures and adjacent tissue layers.

Conclusion: Stokes polarimetry imaging shows that the intervertebral discs and soft tissue regions of rat tails strongly depolarize incident circularly polarized light. Tendon regions remit light with a more linear form due to birefringence. Both DoLP and DoCP image-maps provide contrast between tissue structures. When differentiating between unpolarized light and light with low DoCP or DoLP, the polarization of backscattered light from the turbid medium must be taken into consideration. *Lasers Surg. Med.* 37:396–406, 2005. © 2005 Wiley-Liss, Inc.

Key words: birefringence; near-infrared; scattering

INTRODUCTION

The polarization of light can survive through multiple scattering events in tissue and tissue phantoms [1,2]. The state of polarization can be measured using polarimetry techniques and can be used as a criterion for tissue-type distinction. Basic studies involving polarized light have focused on differences in the optical properties of a medium; specifically, how these properties influence depolarization [3–9]. The polarization properties of light in reflection mode remitted from tissue phantoms, constructed with variations in the optical properties of layers and different thickness of layers, brought further insight to the influence of multiple layers [10]. Investigations into how scatterer structures in birefringent (i.e., porcine tendon, artery, and myocardium) and optically inactive tissue (blood and fat) contributed to the depolarization of a collimated beam of linear or circular polarized light in transmission showed that the individual incident polarization states were depolarized differently [11].

Illumination of tissue with linearly polarized light has been used in a variety of biomedical imaging techniques. The use of crossed polarizers and ratios involving parallel and perpendicular analyzer positions provide investigators with an enhanced view of vasculature [12,13] and superficial tissue [14,15]. Furthermore, multi-wavelength illumination of tissue coupled with crossed linear polarizers and image differencing visualization demonstrated that a deep subsurface object in chicken tissue could be detected [16]. The use of circularly polarized light to illuminate tissue in imaging applications has also been investigated [17–22]. One study showed that images produced by circularly polarized light could be used in an image subtraction algorithm to achieve enhanced contrast between superficial tissue structures [21]. Mueller matrix polarimetry is a technique that relies on arithmetic manipulations of measurements made with formalized combinations of incident polarizations and analyzer types to determine the elements of the Mueller matrix [17,18]. The incident polarizations include left or right circular polarization; the analyzer types include left or right circular analyzers. For tissue imaging applications, Mueller matrix polarimetry was used to make pixel-by-pixel measurements over a region of interest. With additional processing, images representing the sixteen elements of a Mueller matrix were constructed. So far, Mueller matrix imaging polarimetry in the biomedical field has been used to investigate skin conditions [19,20] and stained hepatic biopsies [22].

Although polarized light has been a major research interest in biomedical optics, imaging with unpolarized light is still used in a majority of current diagnostic procedures ranging from minimally invasive surgical procedures to cutaneous inspection. Images acquired with unpolarized light rely on the clinician to recognize color and textural differences that aid in making a diagnosis. In this study, conventional images of embedded rat tails were achieved by illuminating with unpolarized light; however

Contract grant sponsor: NIH; Contract grant number: R01-HD044015.

*Correspondence to: Joseph T. Walsh, Jr., PhD, 2145 Sheridan Road L274, Evanston, IL 60208.

E-mail: jwalsh@northwestern.edu

Accepted 15 August 2005

Published online in Wiley InterScience
(www.interscience.wiley.com).

DOI 10.1002/lsm.20242

these rat-tail images provided limited information about the tissue structure. For example, images of rat-tail tissue embedded at varying depths of turbid gelatin while being illuminated with unpolarized white light or unpolarized near-infrared, as seen in Figure 1a,b, show only the general shape of the rat tail. Figure 1a provides limited depth information but the tendons on the left and right side of the rat tail can be observed when the tail is close to the turbid gelatin surface. Using 940-nm illumination (Fig. 1b) provided greater depth information but individual tissue structures still could not be observed. Rat tails were the tissue of choice for this imaging study because of their varied structural composition yet the structural components were contained within a simple anatomical layout. The various layers of the tail consist of soft tissue, hard bony material, annulus fibrosis, and birefringent tendons—each influencing the polarization state of light remitted. Rat tails are also economical tissue parts that were obtained conveniently in the university laboratory setting.

A Stokes polarimetry imaging technique can be used to differentiate tissue structures by the polarization state of remitted light. Our previous study [23] described a Stokes imaging-polarimetry technique that used incident linear polarized light to obtain degree of polarization image-maps of rat-tail tissue embedded in a turbid medium while varying the incident polarization angle. The relationship between the incident polarization angle and the birefringent nature of the tendons was illustrated by a series of image-maps that showed various aspects of tissue structures within a rat tail.

The purpose of this study is to observe degree of polarization image-maps of rat-tail tissue embedded in a turbid medium when illuminated with near-infrared circularly polarized light. Because circular polarized light can take on two forms—right or left—both are used to construct degree of linear and circular polarization image-maps. We investigate how increasing the depth of the embedded rat tail within the turbid medium will affect the image-maps as well as whether varying the rat-tail geometry and orientation angle with respect to the light

source affect polarization properties of the remitted light. Since a major component of the rat-tail tissue is tendon, this study also presents an opportunity to understand how a birefringent material located within a turbid medium affects degree of polarization image-maps.

The eventual goal in using this Stokes polarimetry imaging technique is to improve visualization of alterations in supporting tissue matrix. Although normal tissue matrix has a predictable and regular structure, matrix alterations are known to occur in many disease states thereby disrupting this structure. The inclusion of circularly polarized light as another imaging parameter allows its selection when visualizing the differences between normal and pathological regions. Creating degree of linear or circular polarization image-maps while illuminating with incident circularly polarized light can indicate regions that may alter circularly polarized light differently than linearly polarized light. There are many diseases where detection of these tissue matrix differences is important; one such example is endometriosis, a disease in which endometrial tissues are found outside the uterine cavity. Surgeons use minimally invasive laparoscope-based imaging techniques to find and excise the endometriotic lesions, but often have difficulty identifying and characterizing the deeper lesions. Most often, confirmation of tissue pathology awaits the post-operative analysis of the sample biopsy. In general, endometrial implants occur within the peritoneal wall and are characterized by a variable degree of fibrosis and a wide range of pigmentations. Hence, the use of Stokes-polarimetry imaging while illuminating with circularly polarized light may provide utility in detecting changes in the tissue matrix collagen structure where lesions implant. Ultimately, this technique may provide clinicians with a better sense of excision locations.

MATERIALS AND METHODS

Tissue Preparation

Rat tails of euthanized adult Sprague–Dawley rats (350–400 g) were harvested immediately post-mortem by

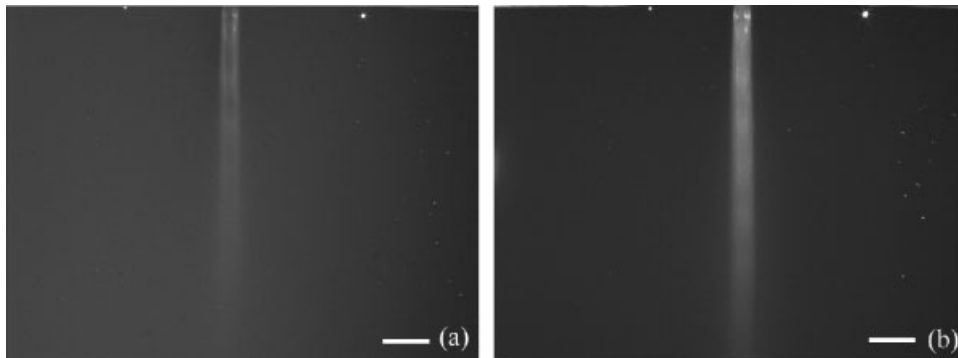


Fig. 1. Image of rat-tail tissue taken while illuminated with (a) unpolarized white light and (b) unpolarized 940-nm light collected without the use of a polarimeter immediately before the camera. Note that only the basic shape of the rat tail can be seen; the more detailed structures are not observed. Bar = 10 mm.

transection at the proximal end. The tails were then frozen. Prior to the polarization imaging experiments, the rat tails were thawed at room temperature for 2 hours. Previous work in our lab has indicated that the freezing/thawing cycle does not affect significantly the birefringence of the rat-tail tendon. The epidermal and dermal layers were dissected away leaving the rat tail tendons, connective tissue, underlying tissue and skeletal structure intact. Each rat tail was suspended inside a plastic container with the tail's long axis at a 15° angle with respect to the bench-top surface. The rat tail position was maintained by two pieces of nylon string: one end of each string attached to the container, the other tied to the tail. A turbid-gel mixture (at 940 nm: $\mu'_s = 0.26/\text{cm}$; $\mu_a = 0.025/\text{cm}$; calculated by following equations described in Farrell et al. [24]; transport mean free path (mfp') = 3.51 cm) consisting of gelatin (Knox; Parisppany, NJ; 5.93 g powdered gelatin/100 ml of H_2O) and non-dairy creamer (Jewel Food Stores; Boise, ID; corn syrup solids, partially hydrogenated soybean and/or canola oils, sodium caseinate, dipotassium phosphate, mono- and diglycerides, silicon dioxide; 8.96×10^{-4} g/ml of H_2O) was used to fill the container and hence embed the tail. The container with the rat tail was refrigerated for 12 hours to solidify the gelatin. The phantom optical properties were selected to form an opaque medium such that the embedded rat tail could be placed at reasonable depths (i.e., on the order of several millimeters) below the gelatin surface and yet when imaging the rat tail with unpolarized visible light the rat tail was not clearly visible. The rat tail was embedded diagonally so that polarization signals could be measured continuously rather than at discrete depths. The tail geometry thus permitted the degree of polarization image-maps to show information at depths up to ~ 20 mm below the gelatin surface. Further, imaging the rat tail embedded at an angle allowed an investigation of the effect of tilt-angle on the polarization-based images.

Polarization Imaging System

Diffuse polarized light illuminated the rat tail embedded in the gelatin and the remitted light was analyzed for its states of polarization. The experimental setup as built in our laboratory is shown in Figure 2. The plastic container with the rat tail embedded in gelatin was placed on top of light-absorbing material. The light source, a fiber-coupled laser (Opto Power Corp.; Tucson, AZ; Model H01-D060-940-FCMS), emitted 940-nm radiation that was directed through a holographic diffuser (Physical Optics Corporation; Torrance, CA; LSDKITCW60-50), a linear polarizer (Corning; Corning, NY; Polarcor 900H-B2), and a quarter-wave plate (Meadowlark Optics, Frederick, CO; AQ-100). To vary the incident circular polarization between right and left circular, the linear polarizer was rotated to the $+45^\circ$ and -45° setting. The light was incident on the gel surface at an angle of 15° from vertical. At this angle of incidence, both the reflectivity of light from the gel surface and the transmission of light into the gelatin did not change significantly for both incident circular polarizations. Nine hundred and forty nanometers of radiation was chosen because of its relatively high penetration depth into tissue.

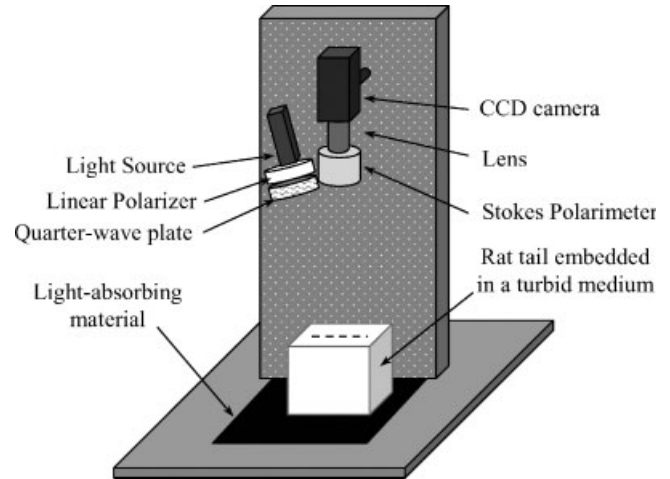


Fig. 2. Schematic diagram of the experimental setup. Unpolarized, 940-nm light from the diode-laser source passed first through a diffuser (not shown), a rotatable linear polarizer, and a quarter-wave plate. The circularly polarized light struck the flat surface of the turbid gelatin at 15° . The rat tail was embedded in the gel at a tip angle of 15° from the horizontal. Remitted light traveling $\pm 1^\circ$ from vertical passed through the Stokes polarimeter and lens to the CCD camera.

The detection optics were set up such that the remitted light traveling within $\pm 1^\circ$ with respect to the vertical axis was collected. The remitted light first passed through a Stokes polarimeter composed of a linear polarizer and a quarter-wave plate, each rotated accordingly to obtain the complete Stokes vectors. A camera lens (Canon; Japan; 100 mm f/13.5) focused the light onto a visible-NIR sensitive CCD (Hitachi; Japan; KP-F120CL; 10-bit resolution, $1,392 \times 1,040$ pixels). Images were transferred to a PC (Dell; Round Rock, TX; Precision Workstation 530) via an image acquisition card (National Instruments; Austin, TX; PCI-1428). Image processing and analysis were carried out using IDL v5.6 (Research Systems, Inc.; Boulder, CO) and Vision Builder v6.1 (National Instruments).

Image Processing and Algorithms

The Stokes parameters were calculated pixel-by-pixel from the images acquired at different analyzer settings. In the Stokes vector, I represents the intensity of the remitted, collected light; Q the difference in intensities between the horizontal and vertical linearly polarized components; U the difference in intensities between linearly polarized components traveling at $+45^\circ$ and -45° with respect to the x-axis; and V the difference in intensities between right and left circularly polarized light [25].

Using the Stokes components, the degree of polarization of the remitted light was calculated:

$$\text{Degree of linear polarization} = \frac{\sqrt{Q^2 + U^2}}{I} \quad (1)$$

$$\text{Degree of circular polarization} = \frac{\sqrt{V^2}}{I} \quad (2)$$

A degree of linear polarization (DoLP) value equal to 1 corresponds to completely linearly polarized light, whereas a degree of linear polarization value equal to 0 corresponds to light with no linear polarization characteristics. A degree of circular polarization (DoCP) value equal to 1 corresponds to completely circularly polarized light, whereas a degree of circular polarization value of 0 corresponds to light with no circular polarization characteristics.

A standard color look-up table (Fire; ImageJ, National Institutes of Health, USA) was applied to the mappings to show the different levels of polarization. The histograms of the mappings were expanded so the levels would make the best use of the color look-up table and display with sufficient contrast. The histogram expansion did not result in any loss of information regarding the polarization properties of the light remitted from the rat tail.

Protocol for Data Collection

Data were collected systematically for both left and right circular incident polarization and various rat-tail orientations. To construct degree of polarization mappings for a specific incident polarization angle, images were acquired

with six analyzer settings. The rat tail was rotated from 0 to 360° in 30° increments. The rat-tail orientation angle (ϕ) is defined as the direction of whichever end the rat-tail was pointing to within the range of 0–180°. For each rat-tail orientation position, the type of incident circular polarization (ICP) was varied between right-circular and left-circular. As a result, 24 different combinations of the ICP and rat-tail orientation angle were investigated. More generally though, because the rat tail was embedded in gelatin at a 15° angle, to completely describe the rat-tail geometry, the rat-tail orientation angle plus the tilt of the rat-tail must be included together. Therefore, as the rat-tail orientation angle was varied, the geometry of the rat tail could be described in three general classifications as shown in Figure 3: tail laying normal to light source (i.e. (a) positioned such that the end of the tail nearest the source was closer to the table top than the opposite end), tail in a neutral position with respect to the light source (i.e. (b) the length-wise position of the rat tail is not preferentially tilted towards or away from the light source), and tail tilted away from the light source (i.e. (c) positioned such that the tail end nearest the source was further from the table top than the opposite end).

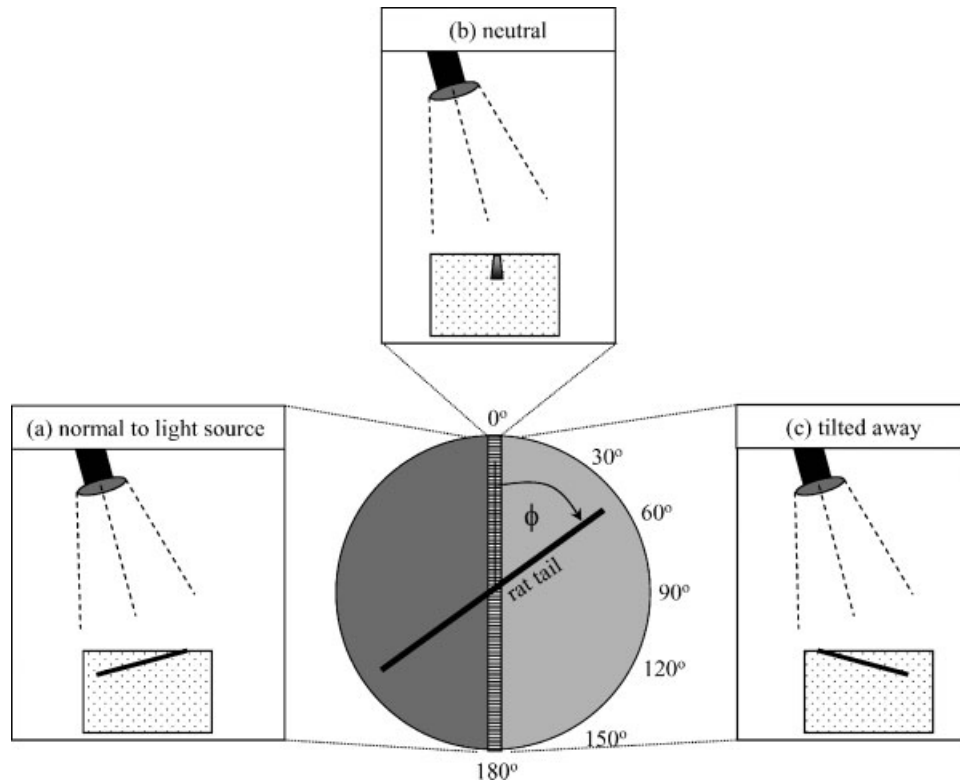


Fig. 3. Rat-tail orientation angle (ϕ) and rat-tail geometry defined with respect to the experimental setup. In this setup, the light source was located to the left of the rat-tail axis of rotation. Rat-tail geometry consisted of three general classifications: (a) rat tail tipped so that it is normal to the light source; (b) tail in a neutral position with respect to light source such that neither the more deeply embedded end nor the near-surface end was tipped away or toward the source ($\phi = 0$ or 180°); (c) tail tilted away from the light source such that the more deeply embedded end was further from the source.

RESULTS

Degree of Linear Polarization Mappings

Various morphologies, which are related to the rat tail anatomy shown in Figure 4, were observed in the DoLP image-maps as the incident circular polarization, the rat-tail orientation angle, and rat-tail geometry were changed. See Figure 5. Three characteristics distinguished the image-maps from each other. These characteristics included the relative strength of the polarization signals from the tendon regions, the high degree of polarization (bright pixels) location, and the presence or absence of banding. In some images, the DoLP for the left and right tendon regions was dissimilar; in other images, the DoLP for these lateral tendons was nearly equal. In all the DoLP image-maps, one observes a banding pattern along the rat tail. This pattern consisted of alternating light and dark regions segmenting the rat tail. The dark regions remitted strongly depolarized light and appeared at locations of the rat tail where the intervertebral discs were located beneath the tendons, as described in Table 1B. These dark regions segmented the tail into multiple sections while the lighter regions highlighted the sections between the discs.

Overall, there was greater linear polarization signal remitted from the rat tail when it was tilted towards the light source (Fig. 5i–n) than when it was either tilted away from the light source (Fig. 5c–h) or in a neutral position (Fig. 5a,b). The bright tendon regions and the banding could be seen to a depth of 18 mm (~ 51 mfp') below the gelatin surface when the rat tail was tilted towards the light source, and to a depth of 15 mm (~ 43 mfp') below the gelatin surface when the rat tail was tilted away from the light source and when the rat tail was in a neutral position. The bright tendon regions corresponded to locations where the tissue layer was arranged as described in Table 1A.

Figure 5b,d,e,g,j show greater signal on the left tendon regions while Figure 5a,h,i show greater signal on the right tendon regions. Similar amounts of signal on bilateral tendon regions were seen in Figure 5c,f,i,k,l,m,n. Between the two parallel tendons regions lay a narrow strip of soft tissue, as described in Table 1C and D. This soft tissue region appeared dark in all the DoLP image-maps and represented an area where the light remitted registered a low degree of linear polarization. These DoLP mappings indicated that the rat-tail orientation angle, rat-tail geometry, and the use of either right or left-circular polarized incident light had an effect on the types of morphologies observed.

Degree of Circular Polarization Mappings

One general morphology was observed for all different rat-tail orientation angles. See Figure 6. In these DoCP image-maps, there was a dark to light gradient along the length of the rat tail; the darker area occurred where the rat tail was closer to the surface and the brighter area occurred where the rat tail was deeper in the turbid medium. Along the long axis of the rat tail, a side-by-side black dashed-stripe appeared at regular intervals. These dark dashed-stripes were longer in the length-wise direction of the rat

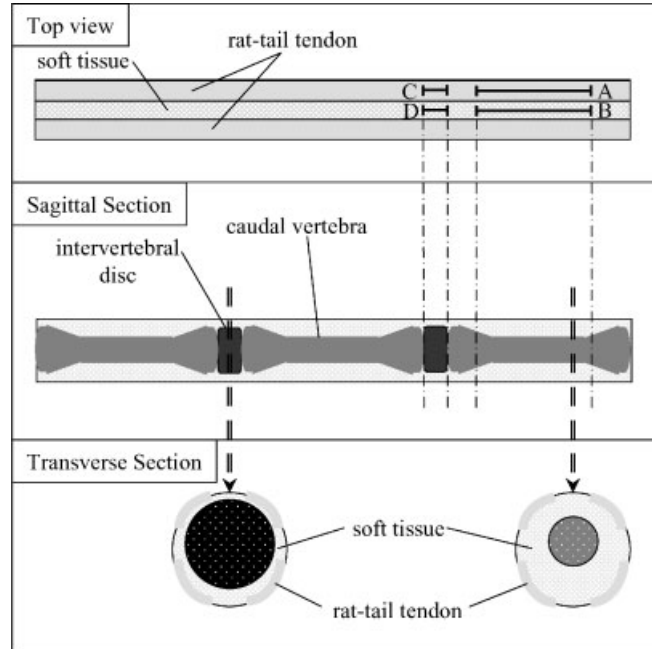


Fig. 4. Illustrations of rat-tail anatomy. Refer to Table 1 for complete descriptions of the regions labeled A, B, C, and D.

tail than in the width-wise direction and corresponded to locations of the tendon that were situated above soft tissue, as described in Table 1A. It was difficult to discern these stripes when the tail was relatively shallow in the gelatin (less than 6 mm (< 0.17 mfp') below the surface). But, as the depth of the rat tail below the surface increased, the stripes became easier to visualize because of the greater contrast (brighter pixels) from the surrounding tissue. At depths greater than 19 mm ($> .54$ mfp') below the gelatin surface, the dashed-stripe pattern was no longer observed.

There were a few small bright spots (~ 1 – 2 mm in diameter) on the rat tail at shallow depths. These spots appeared within the dark regions seen on the rat tail; for example, in Figures 6b,e,f. These spots were most likely a result of very few scattering events and unique locations of the rat-tail tendon that reflected the light into the camera while maintaining most of its circular polarization.

In summary, the DoCP mappings show that for a given rat-tail geometry, the observed morphologies were not dependent upon the rat-tail orientation angle. In addition, the use of either right or left ICP light did not influence the type of morphologies observed.

DISCUSSION

Overview

Circularly polarized light, either present as right or left circular, is characterized by a $\pm \lambda/4$ phase difference between the equal-intensity orthogonal E-field component. The interaction of circularly polarized light with tissue causes these phase differences to be altered; thus, the ellipticity of the propagating and remitted light is changed

according to the polarization-sensitive optical properties of the sample. The DoLP image-maps (Fig. 5) indicate regions of the sample that have converted the incident circular polarization (ICP) state to a more linear form; here, the brighter the pixel is, the greater the conversion. The DoCP image-maps (Fig. 6) indicate regions of the sample that remit light retaining a fraction of the ICP state; here, the

brighter the pixel is, the greater the preservation of the incident polarization. One should note that degree of total polarization image-maps would indicate regions of the sample that remit any type of polarized light (both linear and circular); these image-maps, however, provided no better contrast than DoCP and DoLP image-maps of the rat-tail tissue, and are not shown.

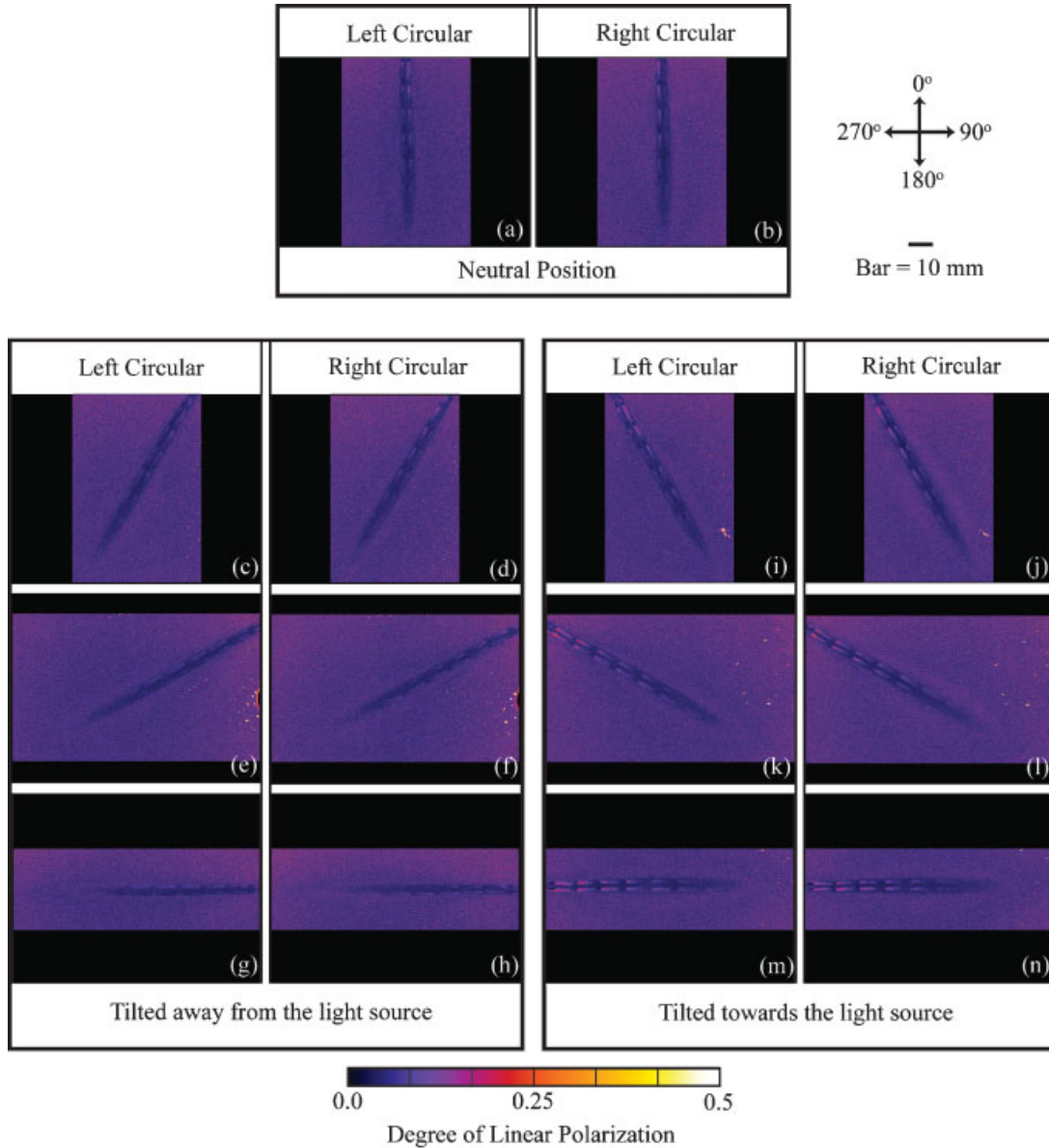


Fig. 5. Several representative degree of linear polarization image-maps for various rat-tail orientation angles and rat-tail geometries created with either left or right incident circular polarized light. There was greater degree of linear polarization remitted from the tendon regions when the rat tail was tilted towards the light source (image-maps **(i–n)**) than when the rat tail was tilted away (image-maps **(c–h)**) or in a neutral position (image-maps **(a–b)**) with respect to the light source. The corresponding rat-tail orientation angles to each of the image-maps are as follows: **(a–b)** $\phi = 0^\circ$; **(c–d)** $\phi = 30^\circ$; **(e–f)** $\phi = 60^\circ$; **(g–h)** $\phi = 90^\circ$; **(i–j)** $\phi = 120^\circ$; **(k–l)** $\phi = 150^\circ$; **(m–n)** $\phi = 90^\circ$. The reference bar indicates a distance of 10 mm. The directional arrows indicate the angles of reference for the rat-tail orientation angles (ϕ).

TABLE 1. Tissue Organization in the Rat Tail and Corresponding Optical and Polarization Properties

	Anatomical arrangement of rat-tail tissue layers	Description of tissue optical and polarization properties
A	Tendon → thick layer of soft tissue → vertebra	Birefringent tissue with an underlying thick layer of soft tissue; the deepest layer consists of highly scattering bone material
B	Tendon → thin layer of soft tissue → intervertebral disc	Birefringent tissue with an underlying thin layer of soft tissue; below this, lies a highly scattering and depolarizing annulus fibrosis
C	Medium-thick layer of soft tissue → vertebra	Soft tissue lies above a highly scattering bone material
D	Thin-layer of soft tissue → intervertebral disc	Soft tissue lies above a highly scattering and depolarizing annulus fibrosis

The DoLP image-maps (Fig. 5) indicate that the birefringence and multiple-scattering events within the turbid medium, rat-tail tendon, and underlying soft tissue caused incident circularly polarized light to be converted to elliptically polarized light, i.e., where the polarization state contained more linear components. Linear birefringence was a major contributing source to these phase changes because of the natural difference in refractive indices along the orthogonal axes of the tendon [25,26].

In short, the conversion of one pure state of polarization, either linear or circular, into elliptically polarized light (i.e., towards a more circular form or towards a more linear form, respectively), is analogous to optical effects created by classical optical components. For example, a retarder or wave-plate can be used to transform linearly polarized light to circularly polarized light or circularly polarized light to linearly polarized light by allowing the light to pass through the optics. In our studies, we have observed similar effects, though not with the exact phase-shifts caused by an engineered wave-plate. Further, the experiments are performed in reflection mode rather than in transmission mode.

In the DoLP image-maps (Fig. 5), the effects due to the tissue layer arrangement shown in Table 1B were observed as dark width-wise bands indicating a relatively low degree of linear polarization. Thus, it appears that the interaction of light with the intervertebral disc did not cause significant conversion of light from circular polarization into a more linearly-polarized form. The outer layer of the intervertebral disc, called the annulus fibrosis, is a laminae composed of fibrous tissue and fibrocartilage. The annulus fibrosis consists of concentric rings of fibers, where each layer of fibers passes in opposite directions. Due to the fibrous nature of this tissue, the polarization state of the remitted light differed from that of the non-fibrous adjacent tissue, where its tissue layer arrangement was described in Table 1A. These differences in the remitted polarization state are what allow this polarimetry-based imaging technique the ability to provide contrast between these subsurface tissue structures. Even with the rat tail embedded within a turbid medium, this imaging technique can detect the subsurface structures of the rat tail (e.g., the intervertebral discs).

The rat-tail geometry influenced how effectively the circularly polarized light was converted into a more linear

form upon remittance. In Figure 6, the amount of conversion is greater when the rat tail was tilted toward the light source or in a neutral position with respect to the light source than when the rat tail is tilted away from the light source. For a birefringent tissue, such as tendon, the results indicate that the angle of incidence with respect to the tissue surface affected the remittance of polarized light. Hence, we believe that a tilt-angle dependence exists such that the coupling of elliptically polarized light into the tendon and remittance of polarized light is more optimal at certain angles of incidence. A detailed goniometric study on tissue tilt-angle could be performed in the future for further characterization of this effect especially for that of tendon.

Asymmetrical Signal Strength

Two other points should be noted from the DoLP image-maps (Fig. 5). First, for certain ϕ 's, there are weaker signals from one side whereas for other ϕ 's the amount of signal is similar from both tendon sides. Second, when the signal strength is dissimilar between the two sides, the use of the left-handed ICP or right-handed ICP caused locations of the dissimilar signals to switch from the left to right side or from the right to left side of the rat tail.

With regards to the first point, the unequal signal strength from either side of the rat tail most probably is attributed to the tendon tilt-angle dependence, as discussed previously. However, in this case, because of natural curvature, the tilt of the tendon is in the lateral direction of the rat tail. Since the tendons along the length of the rat tail were not flat but rather situated on the outside of the cylindrical rat tail, the tendons naturally had slight lateral curvature. Therefore, we hypothesize that the coupling of polarized light into the curved tendon such that a more linear form of polarized light was remitted was not always optimal. At certain ϕ 's, though, both tendons were at tilt-angles such that the coupling into the tendons were optimal resulting in similar amounts of signal from both sides. The variability of the rat-tail diameter may also affect degree of linear polarization remitted. The diameter of a rat tail is larger toward the rostral end and smaller toward the caudal end. Because of the diameter change, there are changes in the curvature along the tail. In this study, however, it was not possible to isolate the individual polarization effects caused by either the curvature

variations or the rat-tail depth because both parameters were changing simultaneously. To fully understand the effects of curvature, a future Stokes polarimetry imaging experiment could be performed on rat tails that are embedded at constant depths below the gelatin surface.

The second point (right vs. left ICP) highlights the significance of the ICP rotational direction. In theory, circularly polarized light has no preferential orientation and so the effect of tendon birefringence on the propagation of circularly polarized light should not be angle dependent

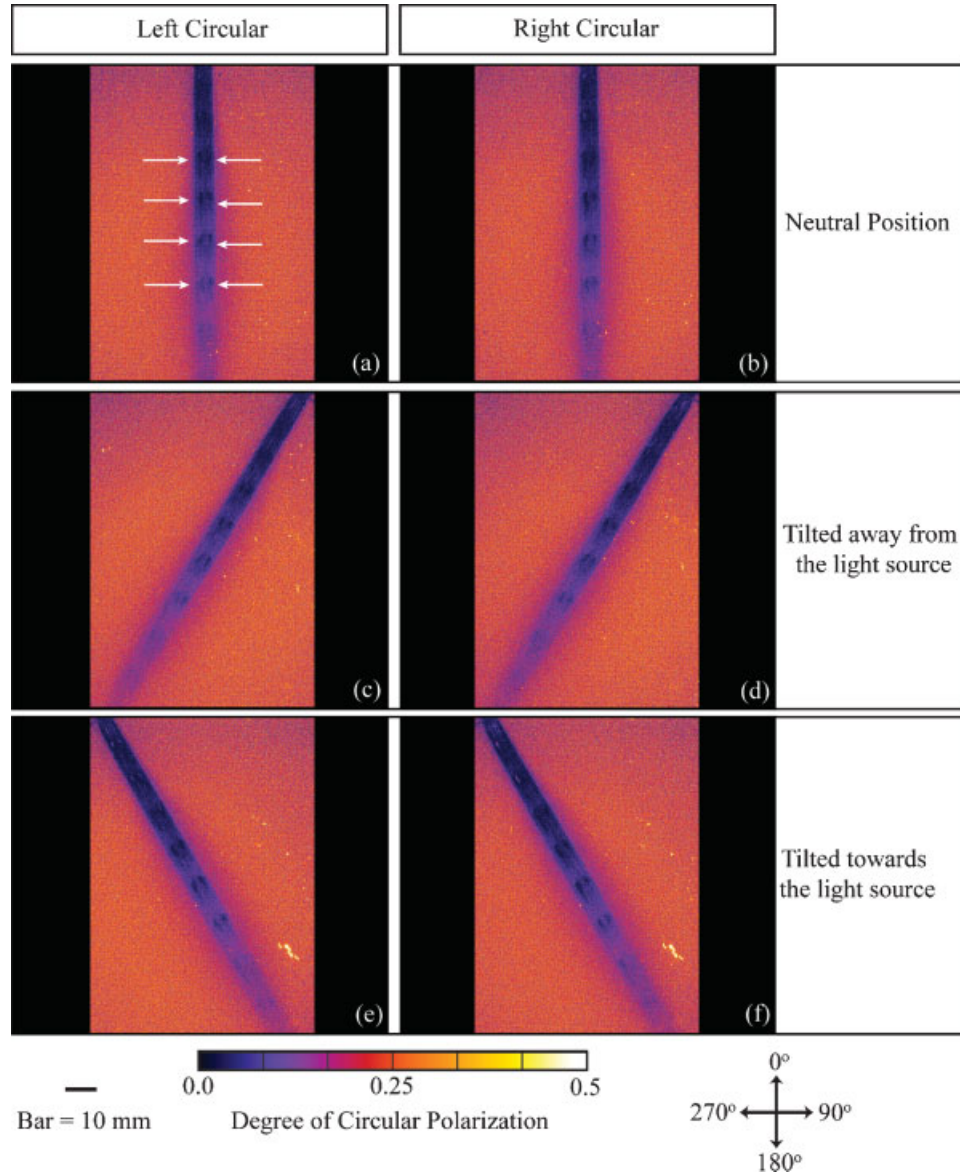


Fig. 6. Several representative degree of circular polarization image-maps for various rat-tail orientation angles and rat-tail geometries created with either left or right incident circular polarized light. All of the image-maps shared the same morphology. In general, there was a dark to bright gradient as the thickness of the turbid medium above the rat tail increased. At depths < 6 mm ($\text{mfp}' < 0.17$), there was little contrast between the tissue structures. A dashed-stripe pattern (indicated by the white arrows in all image-maps) was visible along the length of the rat tail for rat-tail depths between 6 and 18 mm (mfp' between 0.17 and 0.51). The locations of the dashed-stripes corresponded to the tissue layer arrangement described in Table 1A. The corresponding rat-tail orientation angles to each of the image-maps are as follows: (a–b) $\phi = 0^\circ$; (c–d) $\phi = 30^\circ$; (e–f) $\phi = 150^\circ$. The reference bar indicates a distance of 10 mm. The directional arrows indicate the angles of reference for the rat-tail orientation angles (ϕ).

[11]. However, because of diffuse scattering events within the turbid medium, the ICP was no longer purely circular but rather elliptical in nature, especially at greater depths, when incident on the tissue. On the Poincaré sphere, right and left circular polarization are represented on opposite ends of the sphere [18], (Fig. 7). As right or left circularly polarized light undergoes scattering events, its representation on the sphere moves away from the right and left ends of the sphere, respectively, and goes towards the middle of the sphere. Navigating away from either one of these extreme points on the Poincaré sphere (Fig. 7) indicates polarization states that are elliptical and have the same respective handedness, but may have different ellipticities and azimuths. Because the tissue was linearly birefringent, the azimuth parameter had a greater influence than ellipticity on the polarization state of the remitted light. Depending on whether phase was added or subtracted into the left- or right-handed propagating beam, the azimuth of the elliptically light was different. Hence, the alignment of the azimuthal angles with rat-tail orientation angles (ϕ 's) and refraction-indices axes of the birefringent tendons may vary thus causing different levels of DoLP to be remitted from each tendon. In summary, the DoLP image-maps in Figure 5 showed that the conversion of incident circularly polarized light into a more linear form appears to show great sensitivity to a number of material and optical geometrical factors: the tilt-angle of the tissue, the handedness of elliptically polarized light, the azimuth

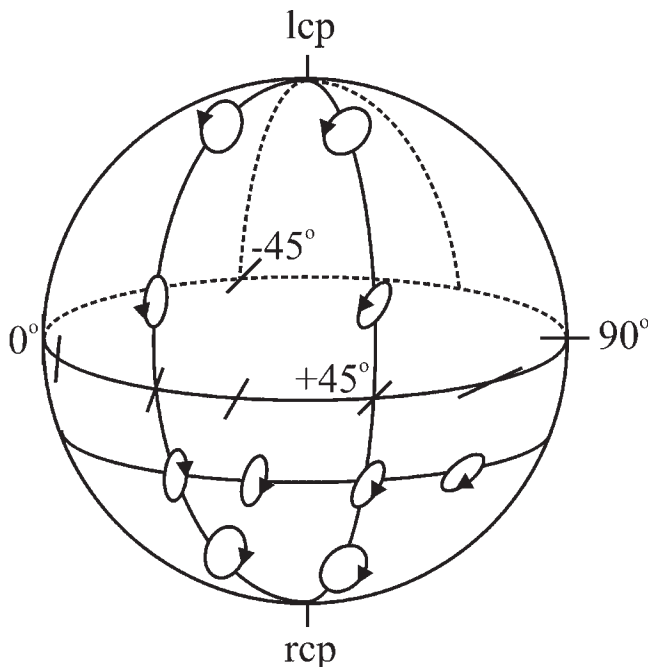


Fig. 7. An illustration of the Poincaré sphere. The x-axis poles are the linear polarization states of 0 and 90°. The y-axis poles are the linear polarization states of 45° and -45°. The z-axis poles are the polarization states of left circular and right circular.

of elliptically polarized light with respect to the rat-tail orientation angle, and the curvature of the tendons.

Effects due to the Turbid Medium Thickness

The common observation in all the DoCP image-maps (Fig. 6) was the general trend of a dark to light gradient along the length of the rat tail. As the thickness of turbid medium above the embedded rat tail increased to over 6 mm (i.e., the mfp' was greater than 0.17), the remitted light from the tissue generally appeared with a lighter shade in the image-maps (i.e., more circular polarization). Because the optical properties of the turbid medium are known and the light remitted immediately from the rat tail retained very little circular polarization (as seen at shallow depths <6 mm ($mfp' < 0.17$)), it was highly unlikely that this gradient was a result of the turbid medium causing remitted light from the tissue to be converted to a more circular form. Hence, there seems to be other effects that caused the observed morphology.

At shallow depths <6 mm ($mfp' < 0.17$), the DoCP image-maps in Figure 6 provided very little contrast between all structures and layers of the rat-tail tissue. There was minimal backscattering from the layer of turbid medium and the rat tail appears as dark pixels. The tendon birefringence together with scattering effects within the rat tail caused the ICP to lose significant amounts of its circular polarization. More specifically though, the tissue regions corresponding to Table 1A converted the polarized light into a more linear form, as observed in the DoLP image-maps (Fig. 5) as bright pixels. Tissue regions corresponding to Table 1B,C,D remitted unpolarized light: unpolarized light is indicated by the appearance of dark pixels in both the DoLP and DoCP (at depths <6 mm ($mfp' < 0.17$)) image-maps at the same general locations. Thus, even though the rat tail appears in the DoCP image-maps (Fig. 6) without contrast and as dark pixels at depths <6 mm ($mfp' < 0.17$), the polarization states of remitted light from the tissue regions (Table 1A,B,C,D) are not the same. Hence, an inherent limitation of DoCP image-maps is its inability to distinguish between unpolarized and linearly polarized light. Similarly, in DoLP image-maps (Fig. 5), unpolarized and circularly polarized light are not differentiated. A dark pixel in either DoLP or DoCP should not be confused with low light intensity; a dark pixel indicates that the detected remitted light was approximately equal in intensity for the analyzer settings used to calculate DoLP or DoCP.

At greater depths (between 6 mm and ~ 18 mm or mfp' between 0.17 and 0.51), the DoCP image-maps (Fig. 6) indicate brighter pixels in the general location of the rat tail. Further, one observes a dashed-stripe pattern running along the length of the rat tail. The dashed-stripe pattern is characterized by a pair of elongated, dark regions (referred to as a pair of stripes) separated by a thin light region between each stripe and a light region both proximal and distal to the pair of stripes. One notes that this pattern is in contrast to the nearly totally dark looking tail found at depths less than 6 mm. One also notes that in regions lateral to the rat tail, i.e., where there is no rat tail, there is a

relatively high DoCP; thus, the turbid gelatin itself backscatters light with significant DoCP. In contrast to the rat tail at shallow depth, where backscatter from the tail contributes significantly to the detected light, when the tail is deeper within the medium, there is fractionally less contribution to the collected light from photons that were remitted from the tail and fractionally more contribution from photons backscattered from the medium. Further, there are regions along the tail that appear either darker or lighter depending upon the polarization state of the light remitted by the rat tail. Tissue regions corresponding to Table 1A do not remit significant DoCP: the dark portion of the dashed-stripe pattern corresponds to the regions remitting linearly polarized light as seen in the DoLP image-maps (Fig. 5). Tissue regions corresponding to Table 1B,C,D appeared to remit light with higher DoCP. The DoCP in these deeper embedded Table 1B,C,D regions is higher in two senses: (1) it is higher than the DoCP in the shallowly embedded rat tail; (2) it is higher than the DoCP in the Table 1A regions.

From the DoLP and DoCP image-maps (Figs. 5 and 6) where the tail was embedded <6 mm below the surface, tissue regions corresponding to Table 1B,C,D remitted mostly unpolarized light, as discussed in a previous paragraph. The data thus indicate that Table 1B,C,D regions more greatly depolarize circularly polarized light than Table 1A regions. Table 1A regions contain birefringent materials that convert the circularly polarized light to a more linear form. For shallowly embedded tails, the difference between the more unpolarized, Table 1B,C,D regions and the more linearly polarized light Table 1A regions is not readily seen—both regions are as dark with low DoCP. For more deeply embedded tails, the difference is greater not because the light interacts differently with the tail but because the overlying medium contributes to the retention of circular polarization and the contribution from unpolarized light remitted from rat-tail regions (corresponding to Table 1B,C,D) does not contribute to the detected Stokes parameters. More specifically, because of the Stokes additivity property¹, the detected Stokes parameters are a sum of beams from both the medium and the tail. Mathematically, unpolarized light has no influence on the detected Stokes parameters as the Stokes representation is $[I, Q, U, V] = [1 \ 0 \ 0 \ 0]$. Therefore, the Stokes parameters of the mostly unpolarized light from the rat tail added to the somewhat polarized light from the turbid medium resulted in a detected signal that was elliptical with moderate DoCP. For the dark portion of the dashed-striped pattern, the presence of some degree of

linear polarization means that parameter(s) Q and U were nonzero, thus the Table 1A region effect contributed to the detected Stokes parameters. Again, by following the additivity property, the Stokes parameters of remitted light from areas corresponding to Table 1A added to those of the backscattered light from the turbid medium results in detected polarization signals that were low in DoCP (i.e., the dark portion of the dash-striped pattern). Of course, to obtain a more complete understanding of the impact of the increasing thickness of the turbid medium on the DoCP and DoLP image maps one would need a measurement of the polarization properties of light incident on the embedded rat tail, an understanding of the affect of the rat tail on light of various ellipticities, and a measurement of the polarization properties of the light remitted from a rat-tail-free medium as a function of the thickness of the turbid medium. Finally, at depths greater than 18 mm ($mfp' > .51$), the scattering effects of the turbid medium became dominant. The impact of the tail is minimal, and the DoCP image-maps (Fig. 6) showed predominantly bright pixels due to the medium without the dashed-stripe pattern.

Relationship to Previous Work

Although previously published works [11,28–30] have described Stokes polarimetry techniques that measure the differences in the propagation of polarized light, these studies did not take the tissue morphology, geometry, and orientation into full consideration. Many of these studies were primarily concerned with varying the microsphere sizes or particle diameters and the tissue morphology, geometry, and orientation were not explicitly studied. In these papers [11,28–30], degree of polarization measurements were made with tissues (e.g., myocardium, artery, tendon) placed in a single orientation. While one incident linear polarization angle or one circular polarization was used to obtain the measurements, this study used both right and left circular incident polarizations. Further, a previous study [24] used various incident linear polarization angles ranging between 0 and 180°. This current study describes a more complete experiment in terms of investigating morphology, geometry, and orientation that influence the degree of polarization. Most importantly, the Stokes polarimetry technique described in the previous literature utilized a narrow beam that propagated through the sample, and measurements were made in transmission. Furthermore, the degree of polarization measurements were made with a single detector such that the scattered light from the bulk tissue was assigned a single value; overall, these methods are fundamentally different than the technique described here. We believe that the imaging component of the current study provides a more complete understanding of how the polarization of light changes after it has interacted with different biological tissue components and scatterers.

Summary

In summary, the experimental data show that degree of polarization measurements are sensitive to changes due to tissue morphology, geometry, and orientation and thus

¹An important property of the Stokes parameters is the property of additivity [28]. If two or more quasi-monochromatic beams propagating in the same direction are superimposed incoherently, the Stokes parameters of the beams can be added and the polarization properties of the combined beam are found by adding the vectors together. When quantifying a Stokes parameter, the actual measurement of irradiance is the sum of the individual beam irradiances. The individual beam irradiances consisted of the individual light packets remitted from the tissue in the backward direction. The beams that were averaged into the degree of polarization measurements were spatially limited by the size of the detector and the lens.

can provide visual contrast between sub-surface tissue structures. Although the application of this technique so far has been limited to investigating ex-vivo tissue and phantoms in a benchtop setting, we believe that the underlying imaging technique shows great promise for medical imaging in the clinic. Pathological or even cancerous tissues are known to have changes within the tissue matrix causing those regions to differ in cellular makeup from normal tissue. One advantage to using this Stokes polarimetry imaging technique is that it provides the ability to scan large regions of tissue efficiently (i.e., during a surgical procedure) while providing important tissue structural information not seen with conventional (unpolarized) optical imaging techniques. The imaging system can just as easily be designed with high magnification to image a much smaller area. This flexibility provides great applicability to various tissues of interest and diagnostic procedures. The suitability of creating DoLP and/or DoCP image-maps should be disease/tissue specific, and can be parameterized as further research is performed. Another distinguishing feature of this imaging technique is that the discrimination of tissue structures is provided by the polarization properties of remitted light rather than by the color appearance or texture of the tissue; this provides an added dimension to viewing differences. In comparison to other imaging techniques, Stokes polarimetry imaging is unique. Optical coherence tomography (OCT) provides excellent microscopic level detail; however scanning large areas (i.e., greater than 10 cm²) is rather inefficient. Furthermore, while both MRI and CT provide excellent anatomical information, they are inadequate in detecting differences within tissue matrix (especially for small lesions) and difficult to adapt to immediate identification and excision procedures.

ACKNOWLEDGMENTS

The authors thank EP, Ltd. for loaning us the 940-nm laser system.

REFERENCES

- MacKintosh FC, Zhu JX, Pine DJ, Weitz DA. Polarization memory of multiply scattered light. *Phys Rev B* 1989; 40(13):9342–9345.
- Studinski RCN, Vitkin IA. Methodology for examining polarized light interactions with tissues and tissue like media in the exact backscattering direction. *J Biomed Opt* 2000; 5(3):330–337.
- Morgan SP, Khong MP, Somekh MG. Effects of polarization state and scatterer concentration on optical imaging through scattering media. *Appl Opt* 1997;36(7):1560–1565.
- Schmitt JM, Gandjbakhche AH, Bonner RF. Use of polarized light to discriminate short-path photons in a multiply scattering medium. *Appl Opt* 1992;31(30):6535–6546.
- Vitkin IA, Studinski RCN. Polarization preservation in diffusive scattering from in vivo turbid biological media: Effects of tissue optical absorption in the exact backscattering direction. *Opt Commun* 2001;190:37–43.
- Hadley KC, Vitkin IA. Optical rotation and linear and circular depolarization rates in diffusively scattered light from chiral, racemic, and achiral turbid media. *J Biomed Opt* 2002; 7(3):291–299.
- Vitkin IA, Hoskinson E. Polarization studies in multiply scattering chiral media. *Opt Eng* 2000;39(2):353–362.
- Hielscher AH, Mourant JR, Bigio IJ. Influence of particle size and concentration on the diffuse backscattering of polarized light from tissue phantoms and biological cell suspensions. *Appl Opt* 1997;36(1):125–135.
- Gurjar RS, Backman V, Perelman LT, Georgakoudi I, Badizadegan K, Itzkan I, Dasari RR, Feld MS. Imaging human epithelial properties with polarized light-scattering spectroscopy. *Nat Med* 2001;7(11):1245–1248.
- Morgan SP, Ridgway ME. Polarization properties of light backscattered from a two layer scattering medium. *Opt Express* 2000;7(12):395–402.
- Sankaran V, Walsh JT, Jr., Maitland DJ. Comparative study of polarized light propagation in biologic tissues. *J Biomed Opt* 2002;7(3):3000–3006.
- Zharov VP, Ferguson S, Eidt JF, Howard PC, Fink LM, Waner M. Infrared imaging of subcutaneous veins. *Lasers Surg Med* 2004;34:56–61.
- Anderson RR. Polarized light examination and photography of skin. *Arch Dermatol* 1991;127:1000–1005.
- Jacques SL, Roman JR, Lee K. Imaging superficial tissues with polarized light. *Lasers Surg Med* 2000;26:119–129.
- Jacques SL, Roman JR, Lee K. Imaging skin pathology with polarized light. *J Biomed Opt* 2002;7(3):329–340.
- Demos SG, Radousky HB, Alfano RR. Deep subsurface imaging in tissues using spectral and polarization filtering. *Opt Express* 2000;7(1):23–28.
- Bickel WS, Bailey WM. Stokes vectors, Mueller matrices, and polarized scattered light. *Am J Phys* 1985;53(5):468–478.
- Collett E. Polarization measurements. In: *Polarized light in fiber optics*. New Jersey: The PolarWave Group; 2003.
- Smith MH, Burke P, Lompado A, Tanner E, Hillman LW. Mueller matrix imaging polarimetry in dermatology. *Proc SPIE* 2000;3911:210–216.
- Baba JS, Chung JR, DeLaughter AH, Cameron BD, Cote GL. Development and calibration of an automated Mueller matrix polarization imaging system. *J Biomed Opt* 2002;7(3):341–349.
- Morgan SP, Stockford IM. Surface-reflection elimination in polarization imaging of superficial tissue. *Opt Lett* 2003;28(2):114–116.
- Laude-Boulesteix B, De Martino AD, Drévilion B, Schwartz L. Mueller polarimetric imaging system with liquid crystals. *Appl Opt* 2004;43(14):2824–2832.
- Farrell TJ, Patterson MS. A diffusion theory model of spatially resolved, steady-state diffuse reflectance for the noninvasive determination of tissue optical properties in vivo. *Med Phys* 1992;19(4):879–888.
- Wu PJ, Walsh JT, Jr. Stokes polarimetry imaging of rat-tail tissue in a turbid medium: Degree of linear polarization image-maps using incident linearly polarized light. *J Biomed Opt* [in press].
- Kliger DA, Lewis JW, Randall CE. *Polarized light in optics and spectroscopy*. San Diego: Academic Press, Inc.; 1990.
- van Blokland GJ, Verhelst SC. Corneal polarization in the living human eye explained with a biaxial model. *JOSA A* 1987;4:82–90.
- Stanworth A, Naylor EJ. Polarised light studies in cornea. I. The isolated cornea. *J Exp Biol* 1953;30:160–163.
- Sankaran V, Walsh JT, Maitland DJ. Polarized light propagation through tissue phantoms containing densely packed scatterers. *Opt Lett* 2000;25(4):239–241.
- Sankaran V, Schonenberger K, Walsh JT, Maitland DJ. Polarization discrimination of coherently propagating light in turbid media. *Appl Opt* 1999, 38(19):4252–4261.
- Sun CW, Lu LS, Yang CC, Kiang YW, Su MJ. Myocardial tissue characterization based on the time-resolved Stokes-Mueller formalism. *Opt Exp* 2002;10(23):1347–1353.